Applied Thermal Engineering 189 (2021) 116669

Contents lists available at ScienceDirect

Applied Thermal Engineering

journal homepage: www.elsevier.com/locate/ate

Research Paper

Plate fin-and-tube heat exchanger computational fluid dynamics model

Karl Lindqvist [a], Geir Skaugen [b], Ole H.H. Meyer [b,*]

[a] Barco, Habornveien 53, NO-1630 Fredrikstad, Norway
[b] SINTEF Energy Research, P.O. Box 4761 Torgarden, NO-7465 Trondheim, Norway

ARTICLE INFO

Keywords:
Numerical modeling
CFD
Fin-and-tube
Thermal–hydraulic correlations
Fin efficiency

ABSTRACT

Insight into thermal–hydraulic correlations of plate fin-and-tube heat exchangers is of great interest in many industrial applications. Numerical simulations allow to efficiently and accurately obtain air-side heat transfer and pressure drop correlations for a broad variety of heat exchanger configurations, provided the numerical method is soundly validated against experimental measurements. In this contribution, we present a thoroughly validated computational fluid dynamics model applicable to solution of the conjugate heat-transfer problem in plate fin-and-tube heat exchangers. Favorable agreement with experimental work on four different geometries is demonstrated for high Reynolds numbers. Three out of four comparisons agree to within 20% with experiments. The computational model is applied to study the dependence of heat transfer and pressure drop in relation to the transverse tube array pitch. We show that minimizing the array angle results in enhanced fin efficiency.

1. Introduction

The fin-and-tube heat exchanger (Fig. 1) is a staple in HVAC&R (Heating, Ventilation, Air Conditioning and Refrigeration) applications, as well as other applications for compact gas-to-liquid heat exchange of vital importance in e.g. power and chemical engineering. The heat exchanger type offers high compactness (large surface area per unit volume) while providing a competitive heat transfer rate per unit pumping power. The latter criterion is critical for most applications involving gas heat exchange, due to the physical properties of gases (e.g. low density leading to large volume flows). It is therefore essential to optimize the heat exchanger geometry for maximum heat transfer per unit pumping power on the gas side.

In many industrial applications, the heat exchanger design is based on empirical knowledge or deduced from experimental correlations. An optimal design in terms of application specific constraints on desired heat transfer rate, maximum pressure drop and footprint is traditionally challenging to obtain. As noted in e.g. [1], empirical correlations for air-side heat transfer and pressure drop in heat exchangers are based on many years of data material, often obtained from heat exchanger and production considerations that have changed today. For instance, more compact design, featuring smaller diameter tubes or thinner fins, may put established correlations outside their validity range, should the functional form of the correlation not respect the flow physics. Correlations deduced from numerical simulations can aid in the process of identifying physical flow features.

Recently, with the aid of rapidly increasing available computational resources, heat exchanger design governed by insight from numerical simulations has become an active field of research.

It is desirable to be able to validate the performance of a thermally optimized design by detailed numerical modeling, before investing in fabrication and experimental testing. Computational Fluid Dynamics (CFD) can supplement experimental measurements and provide additional insights, provided that numerical models are thoroughly validated.

CFD has recently been applied to assess flow phenomena relevant to heat exchanger design. Examples are (not limited to) heat transfer enhancement by helical wires in double pipe heat exchangers [2], fin shaping of plate-and-tube heat exchangers [3], vortex generators in plate-fin heat sinks [4], flow mal-distribution in microchannel heat exchangers [5], and thermal characteristics of compact tube heat exchangers subject to oscillatory flow [6]. Reviews covering the application of CFD methods to heat exchangers are provided in e.g [7,8]. [9] employed the open-source computational fluid dynamics toolbox OpenFoam to validate and demonstrate its conjugate heat transfer capabilities in fin-and-plate and shell-tube heat exchanger geometries. OpenFoam has also been used in [10] to compare conjugate heat transfer modeling with experiments drawn from a single geometry in [11], and constant temperature modeling [12]. Plate-and-fin air-side heat transfer correlations for a fixed geometry have been studied by means of CFD methods in e.g. [13].

* Corresponding author.
E-mail address: ole.meyer@sintef.no (O.H.H. Meyer).

https://doi.org/10.1016/j.applthermaleng.2021.116669
Received 16 September 2020; Received in revised form 4 January 2021; Accepted 29 January 2021
Available online 9 February 2021

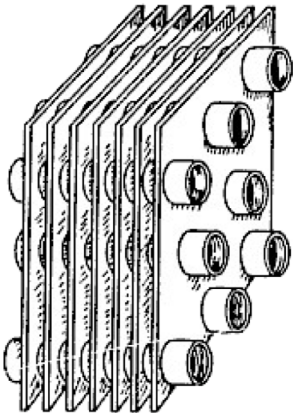

Fig. 1. Fin-and-tube heat exchanger geometry.

Commonly, validation of the CFD method is limited to one particular heat exchanger geometry, and therefore hard to generalize. To this end, this work aims to provide evidence for the accuracy of conjugate heat transfer CFD modeling of fin-and-tube heat exchangers, including possible limitations, by comparing with experiments on four different geometric configurations.

Further, this work seeks to study the influence of the tube array angle (or the ratio of transverse to longitudinal tube pitch) on thermal–hydraulic performance of plain fin-and-tube heat exchangers; a novel application of CFD to heat exchanger modeling. The tube array angle is of significant practical importance, since manufacturing constraints may limit the options available. It is therefore essential to know the thermal–hydraulic trade-off, in order to assess the most feasible practical heat exchanger design.

Fins can be produced in several geometrical variations, e.g. wavy fins, louvered fins or fins with vortex generators. Plain fins, however, are still commonplace due to ease of manufacturing, and allows the tube array angle effect to be separated from possible fin effects.

An effort to condense experimental air-side heat transfer and pressure drop data from fin and tube heat exchangers into correlations that reflect geometrical parameters via the hydraulic tube diameter has been undertaken in [14–16]. Correlations obtained in that fashion including the ratio of characteristic heat exchanger outside and unfinned surfaces, show promising agreement with a number of experimental measurements of air-side heat transfer coefficient and pressure drop. However, detailed parameter dependencies included in the surface areas still need to be worked out.

In this contribution, usefulness of the validated model will be demonstrated by assessing the array angle dependence of the Granryd correlation [17], showing that numerical simulations prove a powerful tool in future heat exchanger design studies.

This article is structured as follows: The model framework, theoretical background, and numerical methodology are outlined in Section 2. Section 3 documents the choice of turbulence model, grid convergence studies and comparison with experiments of different geometry, used to validate the numerical model. The model is then applied to investigate the influence of the array angle on the heat transfer–pressure drop ratio, and compared to the Granryd correlation in Section 4. Finally, conclusions are provided in Section 5.

2. Methodology

In the following, we introduce the computational methodology employed in this work. The conjugate heat-transfer problem at hand, demands solution of the flow field between the tubes, coupled with consistent heat-transfer at the tube surface. Details on the model equations, the numerical framework, computational domain, boundary conditions, thermophysical conditions and the choice of data reduction are presented below.

2.1. Model equations and numerical setup

The flow-field, $\boldsymbol{u}$, is described by the steady-state Reynolds-averaged Navier–Stokes equations,

$$\nabla \cdot (\rho \boldsymbol{u}) = 0, \tag{1}$$

$$\nabla \cdot (\rho \boldsymbol{u} \otimes \boldsymbol{u}) = -\nabla p + \rho \boldsymbol{g} + \nabla \cdot \left[\mu_{\text{eff}} \left(\nabla \boldsymbol{u} + (\nabla \boldsymbol{u})^{\text{tr}}\right)\right], \tag{2}$$

in terms of the (fluid) mass density ρ, pressure p, and the effective viscosity μ_{eff} denotes the sum of molecular and turbulent viscosity. $\boldsymbol{g}$ is the gravitational acceleration vector. Energy continuity is given by,

$$\nabla \cdot (\rho \boldsymbol{u} h_f) + \nabla \cdot (\rho \boldsymbol{u} k) = \nabla \cdot \left(\alpha_{\text{eff}} \nabla h_f\right) + \rho \boldsymbol{u} \cdot \boldsymbol{g}, \tag{3}$$

in terms of the fluid variables specific enthalpy h_f, turbulent kinetic energy $k = \boldsymbol{u} \cdot \boldsymbol{u}/2$, and the effective thermal diffusivity α_{eff} including turbulent thermal diffusivity

$$\alpha_{\text{eff}} = \frac{\kappa_f}{c_{p,f}} + \frac{\rho \nu_{\text{turb}}}{\text{Pr}_{\text{turb}}}, \tag{4}$$

with the fluid thermal conductivity κ_f, specific heat capacity $c_{p,f}$, turbulent viscosity ν_{turb}, and the turbulent Prantdl number Pr_{turb}. The temperature field in the fluid domain is coupled at material walls to the solid domain, where steady state heat conduction is solved

$$\nabla \cdot \left(\frac{\kappa_s}{c_{p,s}} \nabla h_s\right) = 0, \tag{5}$$

with the solid enthalpy h_s, solid thermal conductivity κ_s and solid specific heat capacity $c_{p,s}$. At the fluid–solid interface, continuity of heat fluxes is enforced

$$\kappa \nabla_n T_f = -\kappa_s \nabla_n T_s, \tag{6}$$

where the normal derivative, $\nabla_n = \boldsymbol{n} \cdot \nabla$, and $\boldsymbol{n}$ is an outwards pointing unit vector normal to the wall.

The thermodynamic identity relating fluid enthalpy, entropy (s), and pressure is given by

$$\mathrm{d}h_f = T_f \mathrm{d}s + \mathrm{d}p/\rho, \tag{7}$$

which at constant pressure provides

$$h_f = \int \mathrm{d}T_f c_{p,f}, \tag{8}$$

with the specific heat capacity at constant pressure $c_{p,f} = T_f, (\partial s/\partial T_f)_p$.

The system of equations is closed by a choice of turbulence model. Details are provided in Section 3.1.

2.2. Numerical framework

We use the open-source framework OpenFOAM (version 6) to solve the governing equations. OpenFOAM provides a generic framework for finite-volume discretization of partial differential equations. It is written as a set of C++ libraries, and its object-oriented structure allows for close top-level representation of the mathematical formulations. This enables intuitive custom development and modification [18]. The flexibility of OpenFOAM for tailor-made applications has received increasing attention recently [19].

A typical workflow consists of specifying initial and boundary conditions for the field variables at hand in separate files, as well as mesh files that contain the discretization domain and configuration files to specify the solver with numerical schemes and solution/convergence criteria. Pressure–velocity coupling is solved by the SIMPLE algorithm [20] via the following steps:

1. solve for the velocity vector from the momentum equation with an initial guess of the pressure
2. add corrections to the velocity and pressure
3. solve for the pressure corrections

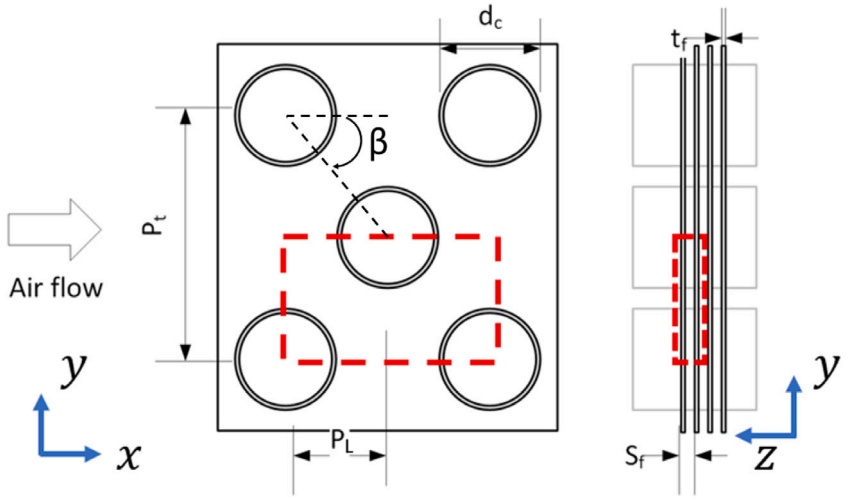

Fig. 2. Fin and tube geometry parameters with computational domain indicated by red dashed lines. d_c, P_t, P_L, S_f and t_f denote tube collar diameter, longitudinal tube pitch, transversal tube pitch, fin pitch and fin thickness, respectively. The array angle is denoted by β. Left: Top view. Right: Side view.

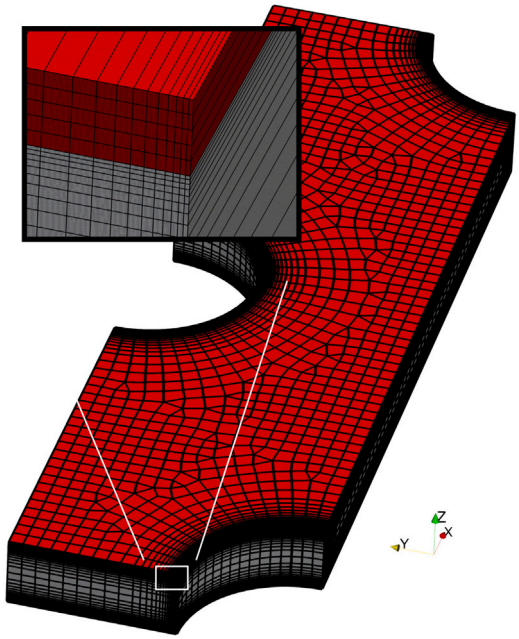

Fig. 3. Computational grid example, red fin domain, gray fluid domain. Bulk fluid cell size is enlarged for clarity.

4. solve for the velocity corrections
5. repeat until the convergence criterion is reached

Interpolation of the face fluxes to the cell values is achieved by combinations of second-order central-differencing schemes. In each iteration, the convergence of velocity, pressure, and enthalpy is monitored. The algorithm is deemed converged upon reaching small enough, user defined, residuals.

Two iterative convergence criteria are used: The drop in mass averaged total pressure ($p_0 + 0.5\rho \boldsymbol{u} \cdot \boldsymbol{u}$) across the computational domain and the total surface heat flux from each fin surface. Equation residuals were also checked for monotonic reduction.

2.3. Computational domain, grid generation and boundary conditions

The computational domain consists of a periodic "unit cell" of the heat exchanger geometry, following the works of Martinez et. al [21] and Lindqvist and Næss [22]. Fig. 2 shows the computational domain in relation to the overall fin-and-tube heat exchanger geometric parameters: The domain is periodic in longitudinal (x) and transversal (y) direction, with respect to the incoming flow (Fig. 2 left), and confined laterally by adjacent fin plates (Fig. 2 right).

2.4. Boundary conditions

The streamwise boundary condition is an adapted version of a strictly periodic (cyclic) boundary condition. Pressure and velocity profiles are sampled from the opposing boundary on regular intervals during the solution process, in a staggered fashion. Remaining fields (temperature and turbulence quantities) are updated every iteration, acting as a fully periodic boundary. This procedure avoids numerical instabilities associated with a fully periodic boundary condition. Uniform boundary profiles are used initially and the boundary condition acts as a prescribed velocity inlet/prescribed pressure outlet between profile updates. Neumann conditions are used for pressure on the inlet boundary and velocity on the outlet boundary, as is common practice. The number of iterations between profile updates are adjusted to ensure convergence. In addition to being copied, profiles for velocity and temperature are scaled to satisfy a specified area average, such that flow rate and temperature difference can be set. Simulations are considered converged when total pressure drop and surface heat fluxes do not change significantly between profile updates, nor with continued iterations.

The combined fluid flow and heat conduction through the fin (conjugate heat transfer) is resolved in the present work. Heat conduction through the fin collar and tube wall, however, is neglected due to its small contribution to the overall thermal conductance [23]. Fin-to-tube contact resistance is neglected for the same reason. The tube surface and the fin root is given a fixed temperature boundary condition of 300 K. Fin surfaces exposed to the fluid uses a coupled boundary condition with a consistent heat flux across the fluid/solid interface.

A 2D quad-dominated hybrid grid is generated in the x-y plane between two adjacent fins and extruded in the z-direction to form the fluid and solid domains (Fig. 3). Half the fin thickness is modeled at each extreme in the z-direction. Sufficient boundary layer resolution,

i.e. $y^+ < 1$ and at least 10 grid points through the boundary layer, is ensured on the tube- and fin surfaces. A boundary layer expansion ratio of 1.12 is used to maintain a smooth transition in cell size throughout the domain. The fin is modeled by 10 cell layers through its thickness.

2.5. Thermophysical conditions

The fluid is modeled as dry air with constant thermophysical properties, including density. This simplification removes the dependency on whether the gas is cooled or heated by the tubes and is justified by the fact that the gas temperature change for each tube row usually is moderate. Even if it is not, the impact on the heat transfer coefficient should be negligible for gas cooling (heat recovery) applications as long as boundary layers remain laminar [24]. As regards the pressure drop, it is common practice to perform measurements in separate, adiabatic, experiments. Hence, the numerical simulations are representative of the experimental setup in this regard. Some thermal–hydraulic correlations indeed correct for the direction of heat flow, but to verify such dependencies is outside the scope of this paper.

The fins are modeled using an isotropic conducting material with constant thermal conductivity corresponding to aluminum ($193\,\mathrm{W\,m^{-1}\,K^{-1}}$) or copper ($390\,\mathrm{W\,m^{-1}\,K^{-1}}$) depending on the experimental setup.

The fluid inside the tubes is not taken into account, i.e. the tube surfaces are kept at uniform temperature, see Section 2.4.

2.6. Data reduction

Upon convergence, the raw data from the numerical model (T,p,U, ...fields) is integrated and reduced to a Reynolds number, a friction factor and a Colburn j-factor to facilitate interpretation and comparison with correlations. The temperature and pressure fields of the fluid are mass flow averaged at the inflow and outflow boundaries as a basis for the data reduction (subscript b). The wall heat flux from the active heat transfer area is evaluated numerically based on Fourier's law and the near-wall fluid temperature gradient.

The fin efficiency is evaluated by computing actual and ideal heat fluxes in separate simulations, for a given flow field, to avoid the restrictive assumptions pertaining to theoretical fin efficiency models. The ideal heat fluxes, Q_{ideal}, are solved by starting from the converged simulation for actual heat fluxes, Q. A frozen flow field is assumed and a uniform temperature boundary condition is applied to all fin surfaces (i.e. infinite thermal conductivity). The fin efficiency is computed as

$$\eta_{\mathrm{f}} = \frac{(\dot{Q}_{\mathrm{f}} + \dot{Q}_{\mathrm{t}})/\Delta T}{(\dot{Q}_{\mathrm{f}} + \dot{Q}_{\mathrm{t}})_{\mathrm{ideal}}/\Delta T_{\mathrm{ideal}}} \tag{9}$$

The Reynolds number based on the tube collar diameter is defined as

$$\mathrm{Re} = \frac{d_{\mathrm{c}} u_{F_{\mathrm{min}}}}{\nu}. \tag{10}$$

The heat transfer coefficient and j factor is calculated as

$$\alpha_{\mathrm{o}} = \frac{\dot{Q}_{\mathrm{f}} + \dot{Q}_{\mathrm{t}}}{[\eta_{\mathrm{f}} A_{\mathrm{f}} + A_{\mathrm{t}}]\Delta T_{LM}}, \tag{11}$$

where ΔT_{LM} is the log mean temperature difference,

$$\Delta T_{LM} = \frac{(T_{\mathrm{b,in}} - T_{\mathrm{t}}) - (T_{\mathrm{b,out}} - T_{\mathrm{t}})}{\ln(T_{\mathrm{b,in}} - T_{\mathrm{t}}) - \ln(T_{\mathrm{b,out}} - T_{\mathrm{t}})}. \tag{12}$$

The Colburn j factor is evaluated as

$$j = \frac{\mathrm{Nu}}{\mathrm{RePr}^{1/3}} = \frac{\alpha_{\mathrm{o}} \mathrm{Pr}^{2/3}}{\rho u_{F_{\mathrm{min}}} c_p}. \tag{13}$$

The Fanning friction factor is calculated based on the difference in mass flow averaged total pressure between the inflow and outflow boundaries, Δp, after [23]:

$$f = \frac{A_{\mathrm{flow}}}{A_{\mathrm{ht}}} \frac{2|\Delta p|\rho}{G_c^2}, \tag{14}$$

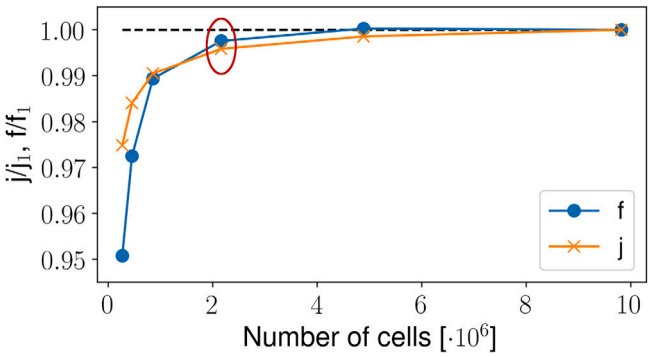

Fig. 4. Results of grid convergence study, with selected grid for production simulations (red circle).

where the $(1 - \sigma^2)$ term is neglected since $\rho_{\mathrm{m}} = \rho_{\mathrm{in}} = \rho_{\mathrm{out}}$ and $G_c = \dot{m}/A_{\mathrm{flow}}$.

3. Grid convergence and validation with experimental data

Grid convergence is tested by generating six different grids with progressively larger bulk fluid cell sizes while keeping $y^+ < 1$ in wall-adjacent cells. The tested bulk fluid cell sizes are in the range 0.059 mm – 0.44 mm. The grid refinement ratio for each step is 1.5 based on cell side length. The grid convergence test uses geometry Wang15 (Table 1).

Results of the grid convergence test show the expected asymptotic convergence of both j and f factors (Fig. 4) with an observed order of accuracy of about 1.7. A bulk fluid cell size of 0.13 mm (marked with red circle) produces results within 0.75% of the finest grid solution, and is judged as a good compromise between accuracy and computational cost.

3.1. Selection of turbulence model

As regards turbulence modeling, the flow in a fin-and-tube heat exchanger remains laminar up to a relatively high Re_{d_c}, as noted by Xie et al. [13]. The turbulent transition point, based on twice the channel height between two fins, depends (by definition) on the fin pitch. Dense geometries may therefore have the entire useful design space in the laminar region. However, for modeling purposes, it is useful to use the same set of model equations for heat exchangers in the laminar and turbulent regimes.

To aid turbulence model selection, two different fin-and-tube geometries are simulated without a turbulence model (assuming laminar flow) and with two different turbulence models: The k-ω SST model [25] and the Spalart–Allmaras model [26]. Both turbulence models can resolve boundary layer profiles down to the viscous sublayer, and hence can be used as low Re models without additional damping functions. Additionally, they do not depend on wall functions. Both models are suitable for boundary layer flows involving adverse pressure gradients.

Results indicate the following:

- The assumption of laminar flow is valid for dense geometries and can be used in the currently considered Reynolds number range, even slightly above the critical Reynolds number for turbulent flow (Fig. 5(a)).
- The CFD model with laminar flow assumption fails to converge for geometries with larger fin pitches (Fig. 5(b)). A possible explanation could be tube wake instabilities that would have to be resolved with a transient simulation.
- The low Re turbulence models give identical results as the laminar model for both fin-and-tube geometries, hence making the laminar model redundant.

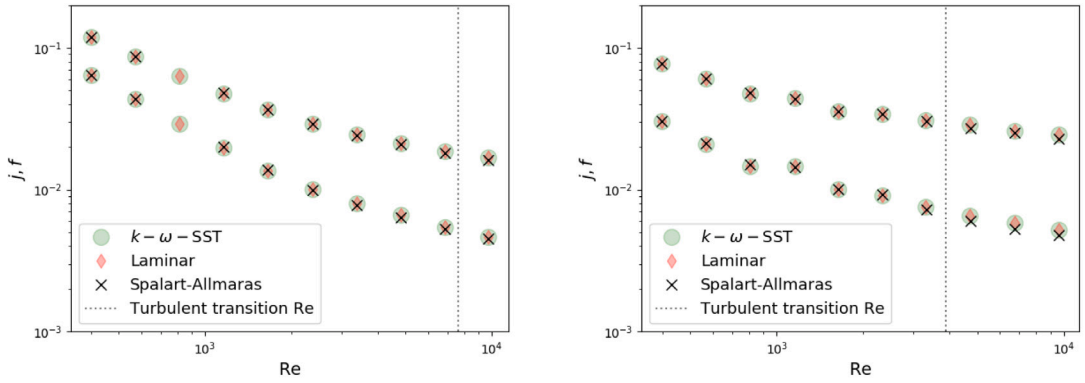

(a) Wang14 geometry (small fin pitch), turbulent transition at Re = 7640.

(b) Wang9 geometry (moderate fin pitch), turbulent transition at Re = 3880.

Fig. 5. Comparison between two different low-Re turbulence models, and a laminar model (no turbulence). Green circles, black crosses and red diamonds denote the $k-\omega-$SST, Spalart–Allmaras, and laminar model, respectively. In both figures, the upper data points represent the friction factor, f, and the lower data points the Colburn j-factor. The vertical dotted lines indicate the turbulent transition Reynolds number.

Table 1
Tube and array geometries (compare Fig. 2).

Geometry	Wang9	Wang14	Wang15	TangP12
Reference	[11]	[11]	[11]	[27]
Fin material	N/A	N/A	N/A	Copper
d_c [mm]	10.23	10.23	10.23	18.6
t_f [mm]	0.13	0.20	0.20	0.30
s_f [mm]	3.16	1.74	3.16	3.1
P_t [mm]	25.4	25.4	25.4	42.0
P_L [mm]	22	22	22	34.0

Table 2
Deviation of numerically and experimentally computed friction- and Colburn j-factor.

Geometry	Wang9	Wang14	Wang15	TangP12
MAE : f	0.007	0.022	0.004	0.004
MAPE : f	14.4%	40.8%	8%	16.8%
MAE : j	0.003	0.014	0.003	0.001
MAPE : j	19%	44.9%	19.6%	9.5%

The k-ω SST model [25] is used throughout the rest of this work based on these conclusions. All turbulence model constants are kept at their default value. A turbulent Prandtl number of 0.85 is used for thermal diffusivity calculations.

3.2. Validation against experiment

Numerical model results are compared with experimental data for the four fin-and-tube geometries given in Table 1. Results are presented in Figs. 6(a)–6(d). The numerical results are also compared with the Granryd correlation, documented in [17] (in Swedish). A comprehensive form of the correlation is also provided in English in the Appendices of [28], however, missing the factor $K_A = 2.39(A_{a,tube}/A_{a,total})^{0.19}$ and the value $K_{z_r} = 1$ for $z_r = 1$ (in their notation).

The numerically computed friction factor and Colburn j-factor are compared with experimental values by means of the mean-absolute-error (MAE) and the mean-absolute-percentage-error (MAPE), given by

$$\mathrm{MAE} = \frac{1}{N}\sum_{i=1}^{N} |Y_{i,\mathrm{num}} - Y_{i,\mathrm{exp}}|, \tag{15}$$

and

$$\mathrm{MAPE} = \frac{1}{N}\sum_{i=1}^{N} \left|\frac{Y_{i,\mathrm{num}} - Y_{i,\mathrm{exp}}}{Y_{i,\mathrm{num}}}\right|, \tag{16}$$

where the subscript "num" indicates a variable from numerical simulations, and "exp" an experimental observation. As the Reynolds numbers from the numerical simulations not necessarily are the same as in the experiments, the MAE is computed for ranges that overlap. For overlapping Reynolds number, the experimental values (means) are interpolated by means of cubic splines, with the interpolation function evaluated at the available Reynolds numbers from the numerical simulations, to produce the quantity Y_{exp}. The error introduced via the cubic spline interpolation is negligible for the purpose of comparison with values from numerical simulations. Resulting absolute errors are presented in Table 2. It should be noted that for the TangP12 geometry, only a single overlapping Reynolds number is used.

Fig. 6 illustrates the overall agreement with the experimental data for the Wang9, Wang15 and TangP12 geometries, particularly at high Reynolds numbers. The numerical model does, on the other hand, under-predict j- and f-factors for the Wang14 geometry substantially (~40%). This geometry has a significantly smaller fin pitch than the other geometries. It is not clear why a small fin pitch would lead to poorer predictive performance. Validation with additional geometries with a small fin pitch is needed.

Moreover, the numerical model does not predict the loss of heat transfer capacity at low Reynolds numbers, as is observed most clearly for the Wang14 geometry. According to Wang et al. [11], the phenomenon is due to a combination of channel flow-like behavior at small fin pitches, and standing vortices that form and fail to break away behind the tubes at low Reynolds numbers. It is possible that transient simulations are required to fully capture these dynamics of the flow numerically.

Finally, comparing the Granryd correlation with experimental data reveals that the correlation is relatively insensitive to the varied geometric parameters. To its credit, the correlation does well match the Reynolds number dependency and produces conservative estimates for f and j without additional safety factors.

4. Numerical results and discussion: Influence of the tube array angle

A parametric study is run to study the effect of tube array angle, β on the heat transfer performance of fin-and-tube heat exchangers. The

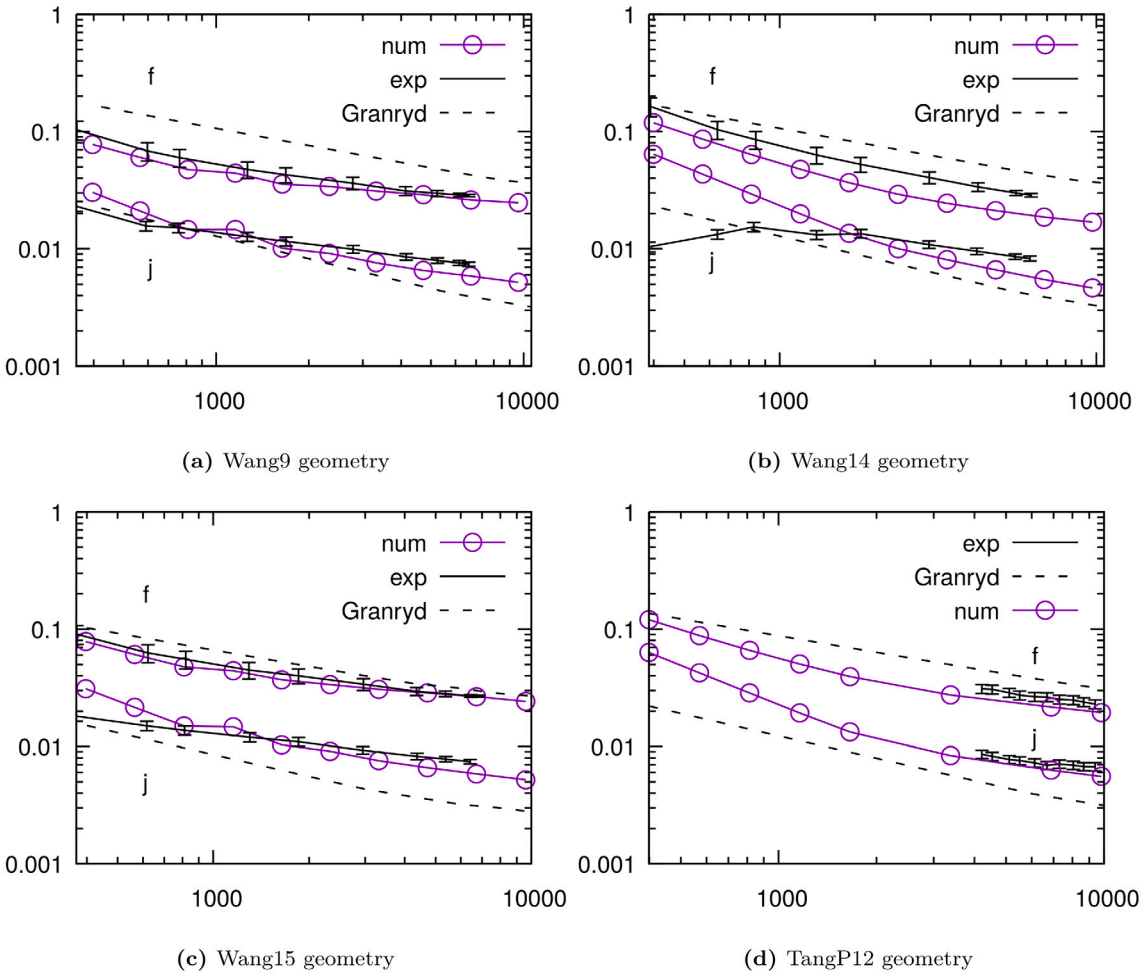

(a) Wang9 geometry (b) Wang14 geometry

(c) Wang15 geometry (d) TangP12 geometry

Fig. 6. Comparison between experimental data, numerical simulations and the Granryd correlation.

array angle is set in terms of the ratio of transverse and longitudinal tube pitch

$$\tan\beta = \frac{P_t}{2P_L}. \tag{17}$$

The transverse tube pitch P_t is varied with the Wang15 geometry as base case with the Reynolds number constant at Re = 4900. Heat transfer performance is quantified by the j/f ratio, the most relevant performance parameter in pressure drop limited applications.

The numerically computed j/f ratio, shown in Fig. 7 as filled circles, initially decreases with array angle down to a minimum at $\beta = 35°$. Thereafter, the j/f ratio recovers somewhat for larger array angles. However, taking the fin efficiency into account, it is clear that the large transverse tube spacing that occur at large array angles is detrimental to fin efficiency (open circles).

A tentative explanation for the observed behavior is that a small transverse tube pitch limits the size of the tube wake and thereby increases the percentage of active heat transfer area. As shown in Fig. 8, the flow at 15° angle is characterized by a small jet (in relation to the tube size) that impinges on the next tube row. The tube wake is limited in size to P_L, and causes good mixing of the flow, leading to a relatively uniform bulk temperature. As the angle is increased to 35°, the tube wake grows and covers a substantial part of the available flow cross section. This, in turn, leads to a high velocity "tube" with large velocity gradients. Finally, at 55°, the flow situation resembles that of an in-line

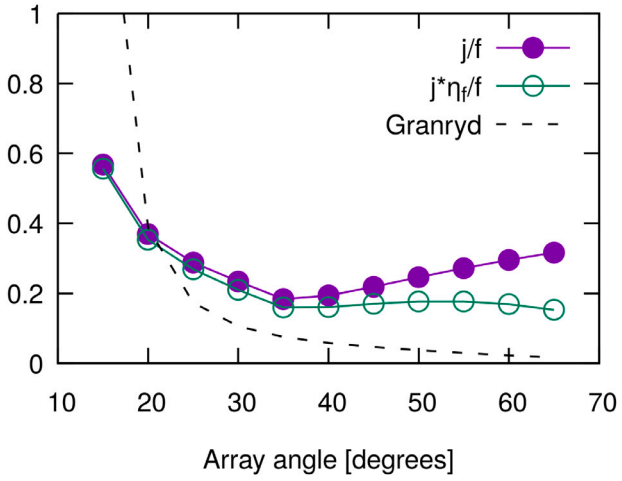

Fig. 7. Effect of tube array angle on the heat transfer performance of Wang15 geometry at Re = 4900. Longitudinal fin pitch held constant.

tube bundle, which is known to be less thermal-hydraulically efficient than a staggered tube bundle.

Comparison of the numerical results with the Granryd correlation indicates that the correlation captures the most important trend,

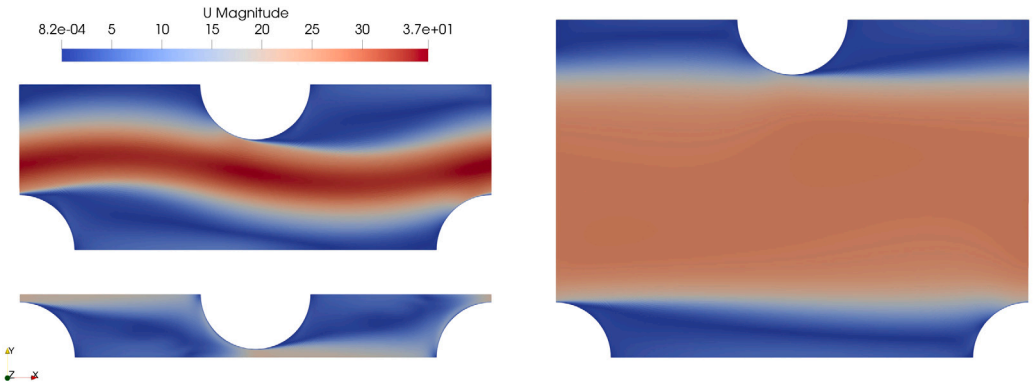

Fig. 8. Velocity magnitude at the mid-plane between two fins, flow from left to right at constant Reynolds number (constant mean velocity) and varying array angle. Lower left: $\beta = 15°$, Top left: $\beta = 35°$, Right: $\beta = 55°$.

namely the increase in j/f with decreased array angle.[1] The increase in j/f at large array angles is not captured, though this trend is of smaller practical importance.

5. Conclusions

This work has presented a numerical model for a semi-infinite fin-and-tube heat exchanger and compared computational results to experimental data for four different heat exchanger geometries. The numerical model is then used to study the influence of the tube bundle array angle on the j/f ratio, indicating pressure drop limited heat exchanger performance. The following conclusions can be drawn:

- From a heat exchanger design perspective, it appears beneficial to minimize the transverse tube pitch as much as possible, within manufacturing constraints, as this increases heat transfer per unit pressure drop.
- Low Reynolds turbulence models appear to produce identical data to a model with a laminar flow assumption. These turbulence models are therefore applicable at all Re, most likely for other heat exchanger geometries as well.
- The numerical model shows agreement to within 20% with experimental data for all but one heat exchanger geometry. It is possible that time-resolved simulations are required to capture all flow dynamics pertinent to fin-and-tube heat exchangers.

The findings should build confidence in the usefulness of CFD analysis, when verification and validation is demonstrated. Further work should, however, resolve the apparent weaknesses in predictive capability at very low Reynolds numbers, and at small fin pitches. Transient simulations will likely provide additional clarity on this issue. Additionally, the proposed method allows to study array angle effects in more detail. This work can be used to study the performance of other correlations outside their original validity regime — an important task to raise confidence in design suggestions from optimization routines.

[1] It should be noted that Granryd's experiments featured $P_t = P_L$ throughout his campaign, however, he also used his correlations for varying P_t at constant P_L [17].

Nomenclature

A_f	fin heat transfer area [m^2]
A_{flow}	minimum free flow area [m^2]
A_{ht}	total heat transfer area [m^2]
A_t	tube heat transfer area [m^2]
c_p	specific heat capacity at constant pressure [$J\,kg^{-1}\,K^{-1}$]
d_o	outer tube diameter [m]
d_c	tube collar diameter ($= d_o + 2t_f$) [m]
G_c	air mass flux based on minimum flow area [$kg\,m^{-2}\,s^{-1}$]
h	specific enthalpy [$J\,kg^{-1}$]
$\boldsymbol{g}$	gravitational acceleration vector [$m\,s^{-2}$]
$\dot{m}$	mass flow [$kg\,s^{-1}$]
$\boldsymbol{n}$	outward pointing unit normal vector [-]
p	total pressure [Pa]
p_0	static pressure [Pa]
P_t	transverse tube pitch [m]
P_L	longitudinal tube pitch [m]
$\dot{Q}$	heat flow [W]
s	specific entropy [$J\,kg^{-1}\,K^{-1}$]
S_f	fin pitch [m]
T	temperature [K]
t_f	fin thickness [m]
$\boldsymbol{u}$	flow velocity vector [$m\,s^{-1}$]
$u_{F_{min}}$	mean velocity in minimum free flow area [$m\,s^{-1}$]
y^+	nondimensional wall distance [-]
f	friction factor [-]
j	Colburn j factor [-]
Pr	Prandtl number [-]
Re	Reynolds number [-]

Greek symbols

α	thermal diffusivity [$m^2\,s^{-1}$]
α_e	apparent heat transfer coefficient [$W\,m^{-2}\,K^{-1}$]
α_o	external heat transfer coefficient [$W\,m^{-2}\,K^{-1}$]
β	tube bundle layout angle [°]
η_f	fin efficiency [-]
κ	thermal conductivity [$W\,m^{-1}\,K^{-1}$]
μ	dynamic viscosity [Pa s]
ν	kinematic viscosity [$m^2\,s^{-1}$]
ρ	mass density [$kg\,m^{-3}$]
σ	contraction ratio of cross-sectional area [-]

Subscripts

avg	average
b	bulk, mixing cup

f fin
f fluid
in inlet
m mean value of inlet and outlet conditions
out outlet
s solid
theotheoretical
turbturbulent

Superscript
tr transpose

Declaration of competing interest

The authors declare that they have no known competing financial interests or personal relationships that could have appeared to influence the work reported in this paper.

Acknowledgments

This publication has been funded by HighEFF - Centre for an Energy Efficient and Competitive Industry for the Future, Norway, an 8-year Research Centre under the FME-scheme (Centre for Environment-friendly Energy Research, Norway, 257632). The authors gratefully acknowledge the financial support from the Research Council of Norway and user partners of HighEFF.

References

[1] C. Bullard, I. Davidson, Extended correlations for staggered round tube plain fin heat exchangers, in: International Refrigeration and Air Conditiong Conference At Purdue, Purdue University, USA, 2006, pp. 1–7.
[2] K. Sharifi, M. Sabeti, M. Rafiei, A. Mohammadi, L. Shirazi, Computational fluid dynamics (CFD) technique to study the effects of helical wire inserts on heat transfer and pressure drop in a double pipe heat exchanger, Appl. Therm. Eng. 128 (2018) 898–910, http://dx.doi.org/10.1016/j.applthermaleng.2017.08.146.
[3] M.-Y. Wen, C.-Y. Ho, Heat-transfer enhancement in fin-and-tube heat exchanger with improved fin design, Appl. Therm. Eng. 29 (2008) 1050–1057, http://dx.doi.org/10.1016/j.applthermaleng.2008.05.019.
[4] S. Fathi, M.E. Yazdi, A. Adamian, Numerical investigation of heat transfer enhancement in heat sinks using multiple rows vortex generators, J. Theoret. Appl. Mech. 58 (2020) 97–108, http://dx.doi.org/10.15632/jtam-pl/115308.
[5] L. Huang, M.S. Lee, K. Saleh, V. Aute, R. Radermacher, A computational fluid dynamics and effectiveness-NTU based co-simulation approach for flow maldistribution analysis in microchannel heat exchanger headers, Appl. Therm. Eng. 65 (2014) 447–457, http://dx.doi.org/10.1016/j.applthermaleng.2014.01.046.
[6] O.M. Ilori, A.J. Jaworski, X. Mao, Experimental and numerical investigations of thermal characteristics of heat exchangers in oscillatory flow, Appl. Therm. Eng. 144 (2018) 910–925, http://dx.doi.org/10.1016/j.applthermaleng.2018.07.073.
[7] M.M.A. Bhutta, N. Hayat, M.H. Bashir, A.R. Khan, K.N. Ahmad, S. Khan, CFD Applications in various heat exchangers design: a review, Appl. Therm. Eng. 32 (2012) 1–12, http://dx.doi.org/10.1016/j.applthermaleng.2011.09.001.
[8] L. Chai, S.A. Tassou, A review of airside heat transfer augmentation with vortex generators on heat transfer surface, Energies 11 (2018) http://dx.doi.org/10.3390/en11102737.
[9] P. Renze, K. Akermann, Simulation of conjugate heat transfer in thermal processes with open source CFD, ChemEngineering 3 (2019) http://dx.doi.org/10.3390/chemengineering3020059.
[10] T. Välikangas, R. Karvinen, Conjugated heat transfer simulation of a Fin-And-Tube Heat Exchanger, Heat Transfer Eng. 39 (2018) 1192–2000, http://dx.doi.org/10.1080/01457632.2017.1363628.
[11] Chi-chuan Wang, Yu-juei Chang, Yi-Chung Hsieh, Yur-Tsai Lin, Sensible heat and friction characteristics of plate fin-and-tube heat exchangers having plane fins transfert de chaleur sensible et caract6ristiques de frottement pour 6changeurs de chaleur plaque-ailettes , pourvus d ' ailettes planes, Int. J. Refrig. 19 (4) (1996) 223–230.
[12] T. Välikangas, Simulation Method Development for Fin-And-Tube Heat Exchanger with Open Source Software, Master's thesis, Tamper University of Technology, Finland, 2015.
[13] Gongnan Xie, Qiuwang Wang, Bengt Sunden, Parametric study and multiple correlations on air-side heat transfer and friction characteristics of fin-and-tube heat exchangers with large number of large-diameter tube rows, Appl. Therm. Eng. 29 (1) (2009) 1–16, http://dx.doi.org/10.1016/j.applthermaleng.2008.01.014.
[14] B.M. Jaćimović, S.B. Genić, B.R. Latinović, Research on the air pressure drop in plate finned tube heat exchangers, Int. J. Refrig. 29 (2006) 1138–1143, http://dx.doi.org/10.1016/j.ijrefrig.2006.02.003.
[15] M. Otović, M. Mihailović, S. Genić, B. Jaćimović, U. Milovančević, S. Marković, Reconsideration of data and correlations for plate finned-tube heat exchangers, Heat Mass Transf. 54 (2018) 2987–2994, http://dx.doi.org/10.1007/s00231-018-2328-0.
[16] M. Mihailović, B. Milovančević, M. Otović, P. Kolendić, Air side heat transfer coefficient in plate finned tube heat exchangers, Exp. Heat Transfer 33 (2020) 388–399, http://dx.doi.org/10.1080/08916152.2019.1656298.
[17] Eric Granryd, Forced Convection Heat Transfer and Pressure Drop in Tube-In-Fin Heat Exchangers, Thesis for the tekn. lic. degree, Kungliga Tekniska Högskolan Stockholm, 1964.
[18] H.G. Weller, G. Tabor, H. Jasak, C. Fureby, A tensorial approach to computational continuum mechanics using object-oriented techniques, Comput. Phys. 12 (6) (1998) 620, http://dx.doi.org/10.1063/1.168744.
[19] H. Jasak, Openfoam: open source CFD in research and industry, Int. J. Nav. Archit. Ocean Eng. 1 (2009) 89–94, http://dx.doi.org/10.2478/IJNAOE-2013-0011.
[20] S.V. Patankar, D.B. Spalding, A calculation procedure for heat, mass and momentum transfer in three-dimensional parabolic flows, Int. J. Heat Mass Transfer 15 (1972) 1787–1806, http://dx.doi.org/10.1016/0017-9310(72)90054-3.
[21] E. Martinez, W. Vicente, M. Salinas-Vazquez, I. Carvajal, M. Alvarez, Numerical simulation of turbulent air flow on a single isolated finned tube module with periodic boundary conditions, Int. J. Therm. Sci. 92 (2015) 58–71, http://dx.doi.org/10.1016/j.ijthermalsci.2015.01.024.
[22] Karl Lindqvist, Erling Næss, A validated CFD model of plain and serrated fin-tube bundles, Appl. Therm. Eng. 143 (2018) 72–79, http://dx.doi.org/10.1016/j.applthermaleng.2018.07.060.
[23] Chi Chuan Wang, Ralph L. Webb, Kuan Yu Chi, Data reduction for air-side performance of fin-and-tube heat exchangers, Exp. Therm Fluid Sci. 21 (4) (2000) 218–226, http://dx.doi.org/10.1016/S0894-1777(00)00005-4.
[24] W.M. Kays, M.E. Crawford, B. Weigand, Convective Heat and Mass Transfer, Fourth, McGraw-Hill Education, New York, 2005, https://books.google.no/books?id=Bo-9QgAACAAJ.
[25] F.R. Menter, M. Kuntz, R. Langtry, Ten years of industrial experience with the SST turbulence model, Turbul. Heat Mass Transf. 4 4 (2003) 625–632, http://cfd.mace.manchester.ac.uk/flomania/pds_papers/file_pds-1068134610Menter-SST-paper.pdf.
[26] P. Spalart, S. Allmaras, A one-equation turbulence model for aerodynamic flows, La Res. Aérospatiale 1 (1994) 5–21.
[27] Ling Hong Tang, Zeng Min, Gong Nan Xie, Qiu Wang Wang, Fin pattern effects on air-side heat transfer and friction characteristics of fin-and-tube heat exchangers with large number of large-diameter tube rows, Heat Transf. Eng. 30 (3) (2009) 171–180, http://dx.doi.org/10.1080/01457630802304253.
[28] P. Verma, C.W. Bullard, P.S. Hrnjak, Design Tool for Display Case Heat Exchanger Frosting and Defrosting, Technical report, University of Illinois at Urbana-Champaign, 2002.